Chapter 1
Introduction

Abstract The structure of the Sun, with its energy generation and heating, creates convection and differential rotation of the outer solar plasma. This convection and rotation generates the solar magnetic field. The field and its variations spawn all of the solar activity: solar active regions, flares, jets, and coronal mass ejections (CMEs). Solar activity provides the origin and environment for both the impulsive and gradual solar energetic particle (SEP) events. This chapter introduces the background environment and some basic properties of SEP events, time durations, abundances, and solar cycle variations.

We tend to think of the Sun as an image of its disk. Recent years have brought increasingly sophisticated images of that disk in single spectral lines and images of active emissions from its corona. However, we have no such images of solar energetic particles (SEPs). In a photon-dominated discipline, SEPs are stealthy and obscure; they do not brighten the solar sky. While photons travel line-of-sight, SEPs are guided out to us along magnetic field lines. We must identify, measure, and count SEPs one by one. Only in recent years have we overcome the limitations so our observations now begin to bear richer fruit. This is the story of that development.

Solar energetic particles (SEPs) come as bursts of high-energy particles from the direction of the Sun lasting for hours or sometimes days. The particle energies range from about 10 keV (kilo electron volts) to relativistic energies of several GeV, particle speeds 90% of the speed of light. In addition to the dominant protons and electrons, most of the other chemical elements from He through Pb have now been measured. The relative abundances of these elements and their isotopes have been a powerful resource in our quest for understanding of the physical processes of acceleration and interplanetary transport of SEPs.

In this chapter we introduce properties of SEPs after reviewing some properties of the solar and interplanetary environment in which they are found.

D.V. Reames, *Solar Energetic Particles*, Lecture Notes in Physics 932,
DOI 10.1007/978-3-319-50871-9_1

1.1 The Structure of the Sun

With a mass of 1.989×10^{33} g, the Sun consists of gaseous, ionized plasma where the inner *core* (see Fig. 1.1) reaches temperatures of 15 million degrees Kelvin (MK) where some of the protons have enough energy to tunnel the Coulomb barrier of the nuclear charge. As they penetrate H, C, and N nuclei, they cause the nuclear reactions that catalyze the conversion of H into He. The energy released in this process is radiated and reabsorbed as it diffuses outward across the *radiative zone*, creating sufficient heat and pressure to balance the gravitational force trying to collapse the star.

Circulation of the hot plasma across the *convection zone* brings energy to the *photosphere*, that surface where overlying material is too thin to absorb radiation or prevent its escape out into space. Here radiation of energy cools the region just above the photosphere to about 4000 K. At this temperature, elements with a first ionization potential (FIP) below about 10 eV, just below that of H at 13.6 eV, remain ionized, while those with higher FIP capture and retain electrons to become neutral atoms.

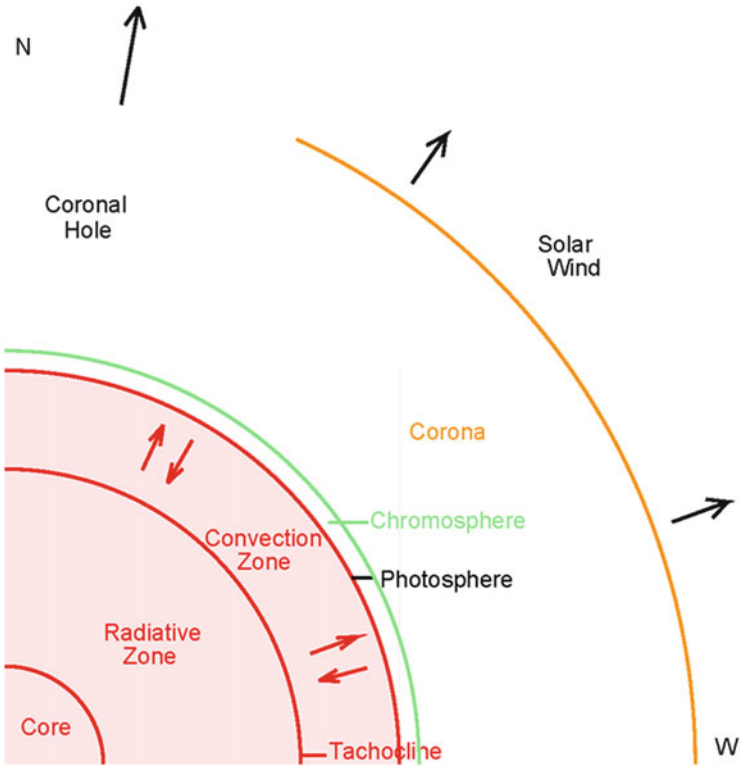

Fig. 1.1 A cross section of the Sun shows its major radial structure from the core to the evaporating solar wind. (If we look at the Sun with North at the *top* and South at the *bottom*, West is to the *right* and East to the *left*. The solar *limb* is the edge of the visible disk.)

Above the photosphere lies the narrow *chromosphere* where the temperature rapidly rises again to over 1 MK in the solar *corona* which extends outward another solar radius or so. The corona is probably heated by absorption of Alfvén waves, plasma waves created in the turbulent layers below, and is largely contained by closed magnetic loops. The outer layer of the corona evaporates to become the 400–800 km s^{-1} *solar wind* which continues to blow past the Earth at 1 AU and far beyond the planets to nearly 100 AU. Properties of the solar wind were predicted by Parker (1963) before it was observed.

Inside the *tachocline*, which lies at the base of the convective zone, the Sun rotates like a rigid body, but throughout the convective zone the Sun rotates *differentially*, faster at the equator than at the poles. The sidereal period of solar rotation at the equator is 24.47 days but it is 25% longer at latitude 60°. Azimuthal surfaces of constant rotation-speed run radially through the convection zone forming conical shells about the rotation axis that extend only to the tachocline and not to their apex at the center of the Sun.

1.2 The Solar Magnetic Field

The Sun has a magnetic field that is generally dipolar in nature, although its origin is still not perfectly understood (see Parker 2009; Sheeley 2005). Magnetic fields, produced in the extreme rotational sheer at the tachocline, are buoyant and produce omega (Ω) loops that rise through the convection zone and emerge through the photosphere to form *sunspots* and *active regions* (Fig. 1.2) as they are sheared and

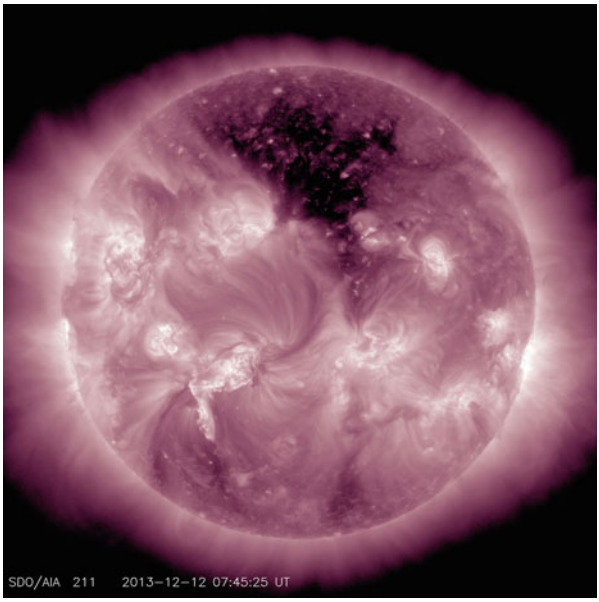

Fig. 1.2 An image of the Sun in 211 Å UV light, taken by the *Atmospheric Imaging Assembly* on the *Solar Dynamics Observatory*, shows brightening of magnetically-complex active regions and a large, dark coronal hole

reconnected by the *differential rotation*. Active regions tend to occur at mid-latitudes on the Sun where the effect of differential rotation on field generation is greatest. When oppositely directed fields reconnect in a largely collisionless regime of the corona, the magnetic energy can be converted to energy of SEPs, with especially copious electrons. On closed magnetic loops, this can result in sudden heating and X-ray production, mainly by electron Bremstrahlung, which is seen as a solar *flare*. Similar reconnection on *open* field lines, *jets*, can release electrons and ions into space, i.e. accelerate an impulsive SEP event, without the trapping or heating, as we shall see. As electrons stream out along open field lines they produce fast-drift type-III radio bursts.

Figure 1.2 shows an image of the Sun in ultraviolet (UV) light taken by the *Atmospheric Imaging Assembly* (AIA) on the NASA spacecraft *Solar Dynamics Observatory* (SDO; http://sdo.gsfc.nasa.gov/). Complex, bright areas in Fig. 1.2 are active regions while the large dark region on the solar image is a *coronal hole*. Coronal holes, often seen near the poles, are regions of *open* magnetic field lines extending into the outer heliosphere, stretched out by the plasma of the solar wind. The bright regions contain locally *closed* field lines, i.e. loops, where any accelerated particles are contained and interact so that heating is greatly increased.

Of course, Maxwell's Equations tell us that *all* magnetic-field lines are *closed*. However, some field lines are drawn far out into the outer heliosphere by coronal mass ejections (CMEs) and the solar wind. For purposes of energetic-particle flow, we describe those field lines as *open* if they can conduct charged particles out from the Sun to an observer at or beyond Earth.

The direction of the solar dipolar magnetic field reverses in a cycle of one reversal in about 11 year and solar activity increases as the field reverses. Solar minima occur when the field axis is aligned with the solar rotation axis, in one polarity or the other, and the number and size of active regions decreases dramatically. Solar maxima occur during intermediate times and the Sun appears as in Fig. 1.2 late in 2013. During solar minimum the northern hemisphere contains nearly radial field lines of one polarity while the southern hemisphere contains the other; the hemispheres are separated by a plane (or wavy) current sheet, between the opposite field polarities, extending out into interplanetary space near the equator. High-speed solar wind (~700–800 km s^{-1}) emerges from the polar coronal holes.

1.3 Coronal Mass Ejections

Magnetic reconnection can lead to the ejection of large filaments containing 10^{14}–10^{16} g mass and helical magnetic field with total kinetic energies of 10^{27}–10^{32} ergs, carrying most of the energy in solar eruptions. CME speeds can be as low as that of the solar wind or can exceed 3000 km s^{-1}. Figure 1.3 shows a large CME imaged by the *Large Angle and Spectrometric Coronagraph* (LASCO) on the *Solar and Heliospheric Observatory* (SOHO; http://sohowww.nascom.nasa.gov/) with a

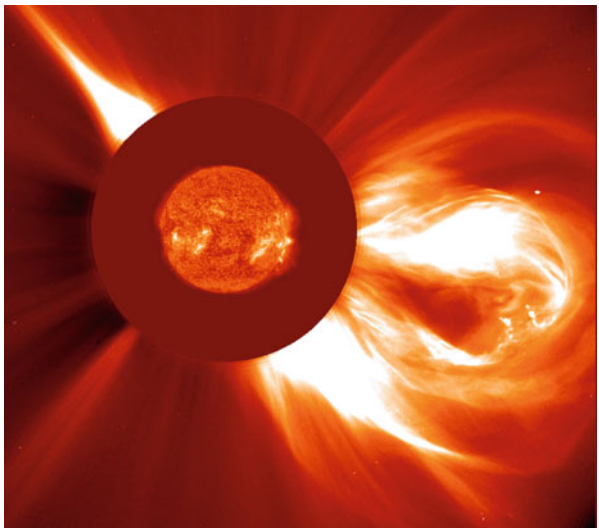

Fig. 1.3 A composite image from the EIT and LASCO telescopes on the NASA/ESA SOHO spacecraft shows a large CME being ejected to the southwest

304 Å image from the *Extreme Ultraviolet Imaging Telescope* (EIT) near the same time scaled onto the coronagraph occulting disk. CME theory and models have been reviewed by Forbes et al. (2006).

Filaments are irregular linear structures of cool, dense, chromospheric plasma magnetically suspended in the corona lying parallel to the solar surface, supported at oppositely-directed magnetic fields beneath an arcade of coronal loops (Martin 1998). They appear dark in Hα images and can hang above the photosphere for days. Filaments that project beyond the solar limb are called *prominences*. Filaments are often ejected as the core of CMEs. In some cases filaments that are present for many days, are suddenly ejected as a CME. These *disappearing-filament* events may drive shock waves and produce SEPs but they lack an associated flare.

When the speed of a CME exceeds the speed of waves in the plasma of the corona or solar wind, it can drive a collisionless shock wave. We will see that fast shock waves are the primary source of acceleration of the largest SEP events.

A bright *streamer* is seen in the upper left (northeast) corner of Fig. 1.3, opposite the CME. Streamers are the magnetic structures stretched behind CMEs after they move out into the heliosphere. As such, they represent newly opening field lines and contribute to the slow (~400 km s^{-1}) solar wind, although the source of the slow solar wind is not fully resolved (e.g. Antiochos et al. 2011). Thus, out-flowing CMEs contribute to the average magnetic field in the heliosphere, which is larger following strong, active solar cycles than weak ones.

1.4 Interplanetary Space

The solar wind expands nearly radially outward from the Sun carrying plasma and magnetic field. The solar-wind speed remains approximately constant with distance from the Sun. As the Sun rotates, the field line connected to a given point on its surface is drawn into a spiral pattern, the Parker spiral. In the inner heliosphere, the plasma density and magnetic-field strength decrease approximately as r^{-2} with distance r, from the Sun, and as $B \sim r^{-1.5}$ by 1 AU (Burlaga 1995, 2001).

Near Earth the typical magnetic field B is ~10 nT, the typical plasma density is ~10 particles cm^{-3}, and the electron plasma frequency, which varies with the electron density, n_e, as $n_e{}^{1/2}$, is ~30 kHz. The solar radius, $R_s = 6.96 \times 10^8$ m = 696 Mm, and the Earth-Sun distance, 1 AU, is 1.50×10^{11} m = 216 R_s, often a useful number. In this spirit, plasma in the 400 km s^{-1} solar wind takes 4.3 days to travel 1 AU, a shock wave with an average speed of 1700 km s^{-1} takes 1 day, a 10 MeV proton or a 5 keV electron takes an hour, and a photon of light takes 8.3 min. Thus, it is not surprising that particles accelerated by a shock wave near the Sun arrive near Earth long before the arrival of the shock itself.

The plasma beta, $\beta_P = \rho kT/(B^2/8\pi)$, where ρ is the density and T the temperature, is the ratio of thermal to magnetic energy density. When $\beta_P < 1$, the field controls the plasma and B is smooth and uniform, when $\beta_P > 1$, the field becomes variable and distorted by plasma turbulence. The internal structure of CMEs is dominated by magnetic field energy, with $\beta_P < 1$.

Alfvén waves propagate through plasma with correlated variations in B and the plasma density ρ with a speed $V_A = B/(4\pi\rho)^{1/2}$. In models of V_A in the solar atmosphere above an active region (e.g. Mann et al. 2003), V_A falls rapidly with height to a value of ~200–500 km s^{-1} at $r \approx 1.5\ R_S$, it then rises to a broad maximum of ~750 km s^{-1} near 4 R_S and finally decays approximately as r^{-1} out toward Earth (Mann et al. 2003) where it is nominally 30 km s^{-1}. However, these values depend upon assumptions about the magnetic structure of an active region. The behavior of V_A is important since the disturbance caused by a CME must exceed the speed of Alfvén waves to form a shock wave which can accelerate SEPs.

Large CMEs can be recognized in the solar wind when they pass Earth (often called ICMEs) and lists of them, with their associated coronagraphic origin, have been published (Richardson and Cane 2010). A class of particularly regular events called *magnetic clouds* is identified by a flux-rope magnetic field that spirals slowly through a large angle (Burlaga et al. 1981). Shock waves driven out by CMEs can also be observed near Earth and their properties can be determined (e.g. Berdichevsky et al. 2000). Lists of properties of interplanetary shock waves spanning many years are available for shocks at the *Wind* and ACE (*Advanced Composition Explorer*) spacecraft (https://www.cfa.harvard.edu/shocks/). We will see examples of shock waves later in this book.

1.5 Solar Energetic Particles

The effort to understand the physical origin of SEP events has led to the identification of two classes of SEP events, *impulsive* and *gradual* with the sources suggested by Fig. 1.4 (e.g. Reames 1999, 2013). The history of this journey will be discussed in Chap. 2 with further physical evidence in Chap. 3. Important differences lie in abundances of elements, isotopes and e/p ratios, as we shall see.

The data base for many measurements from many spacecraft, including SEP intensities, from spacecraft where they were measured, is the Coordinated Data and Analysis Web site: http://cdaweb.gsfc.nasa.gov/sp_phys/. This web site has data from past and current space-physics missions.

1.5.1 Time Duration

While the terms impulsive and gradual did not originally refer to the SEP duration, it is quite often a reasonable characterization as shown by the event series in Fig. 1.5.

1.5.2 Abundances

The abundances of elements and isotopes have been powerful indicators of the origin, acceleration, and transport of SEPs. It was found (Webber 1975; Meyer 1985) that the average element abundances, in events we now call large, gradual SEP events, were a measure of the corresponding solar *coronal* abundances. These differ from abundances in the photosphere by a factor which depends on the first

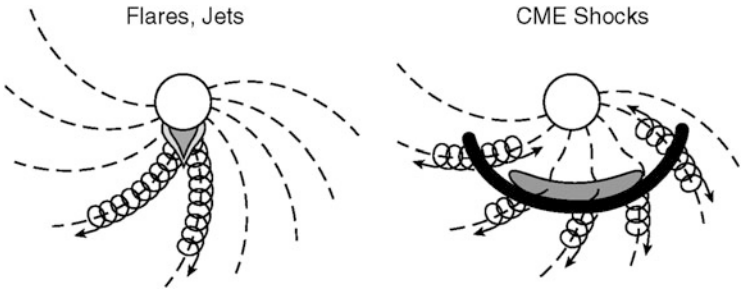

Fig. 1.4 Impulsive (*left*) and gradual (*right*) classes of SEP events are distinguished by the probable sources of particle acceleration in each case (Reames 1999). Impulsive SEP events are accelerated in magnetic-reconnection events on open field lines (i.e. jets) in the corona. Gradual SEP events are accelerated at shock waves (*solid black*) driven out from the Sun by CMEs (*gray*). Particles are shown as spirals along $\boldsymbol{B}$ (*dashed*)

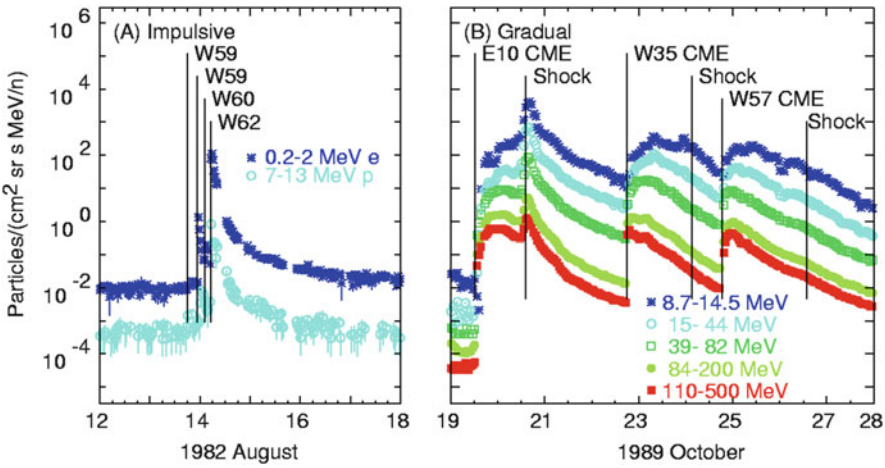

Fig. 1.5 Particle intensities are shown for a series of (**a**) impulsive and (**b**) gradual or long-duration SEP events at similar time and intensity scales. *Flags* labeled with the source longitude indicate the onset times of the events; also shown are the times of shock passage. Proton (or electron) energies are listed. It is difficult to obtain comparable proton energies because impulsive events are much less energetic (Reames 1999)

ionization potential (FIP) of the element as shown in Fig. 1.6 and listed in Table 1.1 (Reames 1995, 2014). Low-FIP elements are ionized in the photosphere while high-FIP elements are neutral atoms. Ions are more easily transported into the corona than are neutrals (e.g. Laming 2009). Other measures of coronal abundances, such as in the solar wind (e.g. Geiss 1982), show a FIP effect that is similar but not identical (Schmelz et al. 2012). These SEP abundances will serve as reference abundances for all discussion of "enhancements" throughout this book.

Table 1.1 lists the photospheric (Asplund et al. 2009) and the reference SEP (Reames 1995, 2014) abundances that we will use. A likely correction to the reference abundance of He (He/O = 91 rather than 57), that will be discussed in Sect. 5.9, is shown as a red open circle in Fig. 1.6. Alternative photospheric abundances by Caffau et al. (2011) make some difference in the FIP plot as demonstrated by Reames (2015); the differences depend on the choice of spectral lines used to obtain the photospheric abundance measurements.

Abundances also distinguish *impulsive* SEP events. The earliest of these was the greatly enhanced ^{3}He/^{4}He ratio, which is ~5×10^{-4} in the solar wind, but can be >1 in impulsive SEP events, as seen in the examples in Fig. 1.7.

These two events have event-averaged Fe/O = 1.24 ± 0.28 and 1.34 ± 0.20, respectively, compared with the reference value of 0.131 ± 0.006 in Table 1.1. Enhancements of even heavier elements (e.g. $Z > 50$) are much greater, on average, but are difficult to measure in single small events and will be seen in Sect. 4.5.

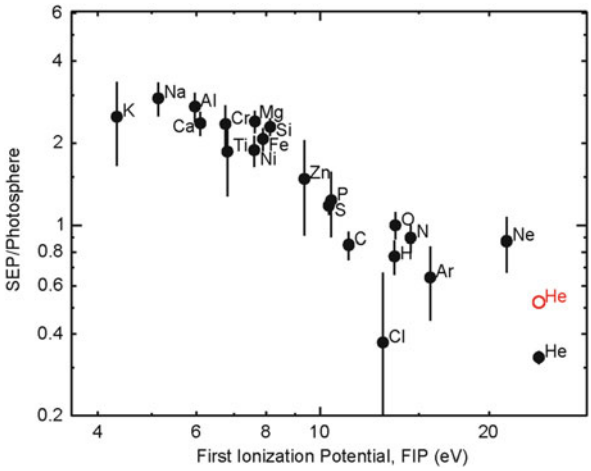

Fig. 1.6 The average element abundance in gradual SEP events (Reames 1995, 2014), or reference abundance, relative to the corresponding abundance in the solar photosphere (Asplund et al. 2009) is plotted as a function of the FIP of the element (see text)

Table 1.1 Photospheric and SEP-reference abundances used in Fig. 1.6

	Z	FIP [eV]	Photosphere	SEP Reference
H	1	13.6	$(2.04 \pm 0.05) \times 10^6$	$(\sim 1.57 \pm 0.22) \times 10^6$
He	2	24.6	$(1.74 \pm 0.04) \times 10^5$	$57{,}000 \pm 3000$
C	6	11.3	550 ± 63	420 ± 10
N	7	14.5	138 ± 16	128 ± 8
O	8	13.6	1000 ± 115	1000 ± 10
Ne	10	21.6	174 ± 40	157 ± 10
Na	11	5.1	3.55 ± 0.33	10.4 ± 1.1
Mg	12	7.6	81 ± 8	178 ± 4
Al	13	6.0	5.75 ± 0.40	15.7 ± 1.6
Si	14	8.2	66.1 ± 4.6	151 ± 4
P	15	10.5	0.525 ± 0.036	0.65 ± 0.17
S	16	10.4	26.9 ± 1.9	25 ± 2
Cl	17	13.0	0.65 ± 0.45	0.24 ± 0.1
Ar	18	15.8	5.1 ± 1.5	4.3 ± 0.4
K	19	4.3	0.22 ± 0.14	0.55 ± 0.15
Ca	20	6.1	4.47 ± 0.41	11 ± 1
Ti	22	6.8	0.182 ± 0.021	0.34 ± 0.1
Cr	24	6.8	0.89 ± 0.08	2.1 ± 0.3
Fe	26	7.9	64.6 ± 6.0	131 ± 6
Ni	28	7.6	3.39 ± 0.31	6.4 ± 0.6
Zn	30	9.4	0.074 ± 0.009	0.11 ± 0.04

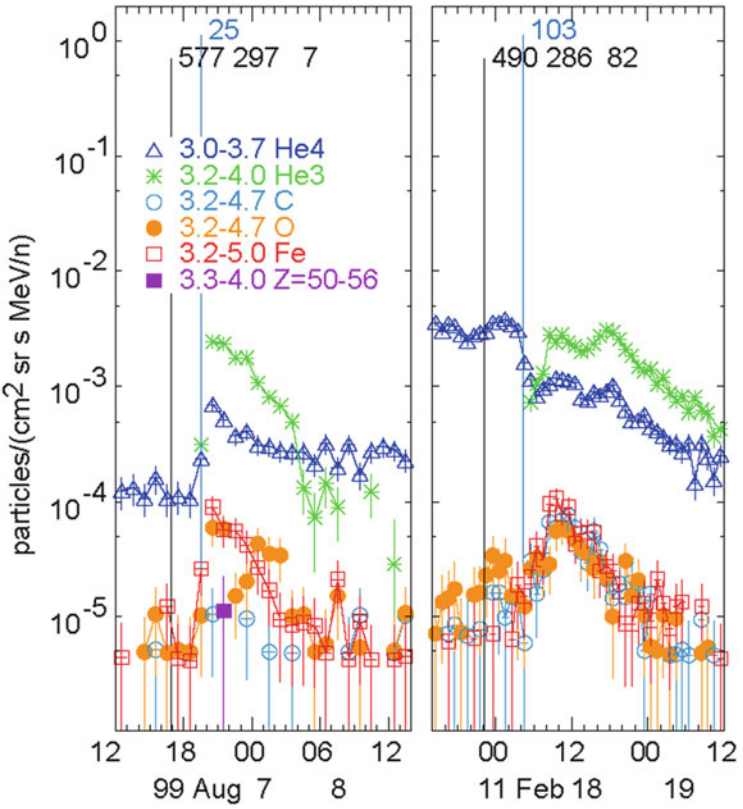

Fig. 1.7 Intensities vs. time are shown in impulsive SEP event numbers 25 and 103 (shown in blue flags at event onsets) from Reames et al. (2014). ^{3}He exceeds ^{4}He in these events and Fe exceeds C and O. Flags in black preceding the SEP onsets are at the associated CME onset times and list the speed (km s^{-1}), position angle (deg), and width (deg) of the CME

1.5.3 The Solar Cycle

SEP events do not precisely follow the solar activity level of sunspots, but they do have a definite solar cycle. The upper panel of Fig. 1.8 shows intensities of 120–230 MeV protons measured by the *Goddard Space Flight Center* telescope on the IMP-8 (*Interplanetary Monitoring Platform*) spacecraft. This telescope is sensitive to particles of solar and galactic origin and can observe the counter-cyclical behavior. When the Sun is active with SEP events, the greater ejection of CMEs increases the modulation that blocks and decreases the encroachment of galactic cosmic rays. The monthly sunspot number is shown in the lower panel for comparison.

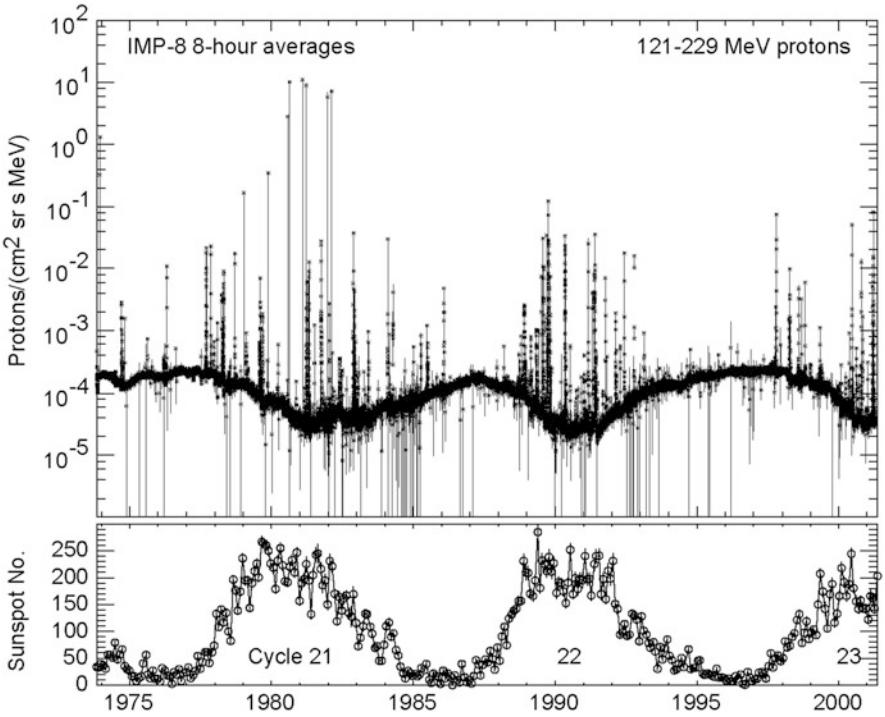

Fig. 1.8 Intensities of 120–230 MeV protons in 8-h averages from the Goddard IMP-8 telescope are shown over 27 years in the upper panel. Spikes from individual SEP events reach a factor of 10^5 above a counter-cyclical baseline of galactic cosmic rays which the instrument also measures well. The monthly international sunspot number is shown in the lower panel for comparison

1.5.4 Relativistic Kinematics

What we often call the particle "energy," E commonly quoted as MeV amu^{-1} is actually a measure of velocity $E = \mathcal{E}/A = M_u(\gamma - 1) \approx \frac{1}{2} M_u \beta^2$, where $\mathcal{E}$ is the total kinetic energy, A is the atomic mass, $M_u = m_u c^2 = 931.494$ MeV, $\gamma = (1-\beta^2)^{-1/2}$, and $\beta = v/c$ is the particle velocity relative to the speed of light, c. Abundances of elements and isotopes are always compared at the same value of E. The total energy of a particle is $W = AM_u\gamma$ and the momentum is given by $pc = AM_u\,\beta\gamma$. The magnetic rigidity or momentum per unit charge is $P = pc/Qe = M_u\,\beta\gamma\,A/Q$ in units of MV. Note that the atomic mass unit (amu), 1/12 the mass of ^{12}C, is close enough to nucleon masses that MeV nucleon^{-1} is indistinguishable from MeV amu^{-1} for SEP studies.

We can write the Lorentz force on a single particle in the form

$$m_u \frac{d}{dt}(\gamma\ \mathbf{v}) = \frac{Q}{A} e(\mathbf{E} + \mathbf{v} \times \mathbf{B}) \tag{1.1}$$

In a collisionless world where the electric and magnetic fields are independent of the nature of the particle, the only specific particle species dependence is Q/A. This will be the case for most of the wave-particle interactions we will encounter during particle acceleration and transport. The exception comes when the particle interacts with matter where the electric field is that of the particle itself and depends upon Q as it scatters electrons of the stopping material. This is the case in particle detectors (Chap. 7) where the species-dependence for energy loss becomes Q^2/A. Strong enhancements observed in elements with $76 \leq Z \leq 82$ in impulsive SEPs would have been suppressed by this dependence on Q^2/A if the ions had traversed significant amounts of matter during acceleration or transport. Thus, acceleration and transport are essentially collisionless and depend upon Q/A.

Acknowledgements We thank the SOHO and SDO projects for figures used in this chapter.

References

Antiochos, S.K., Mikić, S., Titov, V.S., Lionello, R., Linker, J.A.: A Model for the sources of the slow solar wind. Astrophys. J. **731**, 112 (2011)

Asplund, M., Grevesse, N., Sauval, A.J., Scott, P.: The chemical composition of the sun. Annu. Rev. Astron. Astrophys. **47**, 481 (2009)

Berdichevsky, D.B., Szabo, A., Lepping, R.P., Vinas, A.F., Mariana, F.: Interplanetary fast shocks and associated drivers observed through the 23rd solar minimum by Wind over its first 2.5 years. J. Geophys. Res. **105**, 27289 (2000). Errata in J. Geophys. Res., **106**, 25133, (2001)

Burlaga, L.F.: Interplanetary Magnetohydrodynamics. Oxford University Press, Oxford (1995)

Burlaga, L.F.: Magnetic fields and plasmas in the inner heliosphere: Helios results. Planet. Space Sci. **49**, 1619 (2001)

Burlaga, L.F., Sittler, E., Mariani, F., Schwenn, R.: Magnetic loop behind an interplanetary shock: Voyager, Helios, and Imp 8 observations. J. Geophys. Res. **86**, 6673 (1981)

Caffau, E., Ludwig, H.-G., Steffen, M., Freytag, B., Bonofacio, P.: Solar chemical abundances determined with a CO5BOLD 3D model atmosphere. Sol. Phys. **268**, 255 (2011). doi:10.1007/s11207-010-9541-4

Forbes, T.G., Linker, J.A., Chen, J., Cid, C., Kóta, J., Lee, M.A., Mann, G., Mikic, Z., Potgieter, M. S., Schmidt, J.M.: CME theory and models. Space Sci. Rev. **123**, 251 (2006)

Geiss, J.: Processes affecting abundances in the solar wind. Space Sci. Rev. **33**, 201 (1982)

Laming, J.M.: Non-WKB models of the first ionization potential effect: implications for solar coronal heating and the coronal helium and neon abundances. Astrophys. J. **695**, 954 (2009)

Mann, G., Klassen, A., Aurass, H., Classen, H.-T.: Formation and development of shock waves in the solar corona and the near-Sun interplanetary space. Astron. Astrophys. **400**, 329 (2003)

Martin, S.F.: Conditions for the formation and maintenance of filaments (invited review). Sol. Phys. **182**, 126 (1998)

Meyer, J.P.: The baseline composition of solar energetic particles. Astrophys. J. Suppl. **57**, 151 (1985)

Parker, E.N.: Interplanetary Dynamical Processes. Interscience, New York (1963)

Parker, E.N.: Solar magnetism: the state of our knowledge and ignorance. Space Sci. Rev. **144**, 15 (2009)

Reames, D.V.: Coronal abundances determined from energetic particles. Adv. Space Res. **15**(7), 41 (1995)

Reames, D.V.: Particle acceleration at the Sun and in the Heliosphere. Space Sci. Rev. **90**, 413 (1999)
Reames, D.V.: The two sources of solar energetic particles. Space Sci. Rev. **175**, 53 (2013)
Reames, D.V.: Element abundances in solar energetic particles and the solar corona. Sol. Phys. **289**, 977 (2014)
Reames, D.V.: What are the sources of solar energetic particles? Element abundances and source plasma temperatures. Space Sci. Rev. **194**, 303 (2015)
Reames, D.V., Cliver, E.W., Kahler, S.W.: Abundance enhancements in impulsive solar energetic-particle events with associated coronal mass ejections. Sol. Phys. **289**, 3817 (2014). doi:10.1007/s11207-014-0547-1
Richardson, I.G., Cane, H.V.: Near-Earth interplanetary coronal mass ejections during solar cycle 23 (1996-2009): Catalog and summary of properties. Sol. Phys. **264**, 189 (2010)
Schmelz, J.T., Reames, D.V., von Steiger, R., Basu, S.: Composition of the solar corona, solar wind, and solar energetic particles. Astrophys. J. **755**, 33 (2012)
Sheeley Jr., N.R.: Surface evolution of the sun's magnetic field: a historical review of the flux-transport mechanism. Living Rev. Sol. Phys. **2**, 5 (2005)
Webber, W.R.: Solar and galactic cosmic ray abundances—a comparison and some comments. Proc. 14th Int. Cos. Ray Conf. Munich. **5**, 1597 (1975)